RESEARCH ARTICLE | FEBRUARY 29 2024

Growth of conformal TiN thin film with low resistivity and impurity via hollow cathode plasma atomic layer deposition

Special Collection: Atomic Layer Deposition (ALD)

Ha Young Lee; Jeong Hwan Han ; Byung Joon Choi

Check for updates

View Online   Export Citation   CrossMark

19 March 2024 01:10:25

Growth of conformal TiN thin film with low resistivity and impurity via hollow cathode plasma atomic layer deposition EP

Ha Young Lee, Jeong Hwan Han, [iD] and Byung Joon Choi[a) [iD]

AFFILIATIONS

Department of Materials Science and Engineering, Seoul National University of Science and Technology, Seoul 01811, Republic of Korea

ABSTRACT

Copper has been used as an interconnect material in integrated semiconductor devices because of its excellent conductivity, mechanical strength, and electromigration resistance. Introducing a diffusion barrier layer using transition metals such as Ti, Ta, W, Mo, and their nitrides can effectively prevent copper diffusion into the transistor region. TiN is widely used as the diffusion barrier. Plasma-enhanced atomic layer deposition (PEALD), which uses plasma to activate molecular reactions, can be used to fabricate high-quality thin films at lower temperatures than thermal atomic layer deposition. However, its high electrical resistivity and poor step coverage are disadvantageous for its adoption in highly scaled three-dimensional structures. In this study, TiN thin films were fabricated using PEALD with a hollow cathode plasma (HCP) source. The fabricated TiN exhibited a high density (5.29 g/cm^3), which was very close to the theoretical density of TiN. Moreover, it has low electrical resistivity (132 $\mu\Omega$ cm) and excellent step coverage (>98%) in a trench pattern with a high aspect ratio of 32:1. These results suggest the possible application of the PEALD of TiN films using HCP sources in semiconductor device manufacturing.

I. INTRODUCTION

Copper has gained attention as a metal interconnect material because of its low electrical resistance and excellent resistance to electromigration compared with aluminum.[1–7] However, copper has two limitations that must be addressed. The first is its poor adhesion to SiO$_2$, owing to its inability to reduce SiO$_2$, resulting in a simple physical bond rather than a chemical bond at the interface. The second mechanism involves rapid diffusion of copper atoms into Si and SiO$_2$. Copper diffuses rapidly into Si even at temperatures below approximately 200 °C and reacts rapidly with Si to form CuSi$_3$, which forms harmful trap levels inside the bandgap, negatively affecting the reliability characteristics of semiconductor devices.[1,2,5–7] To solve these problems, copper diffusion barrier films, such as Ti, Ta, W, TiN, TaN, WN, and MoN, are required between silicon-based devices and copper.[6–12]

With the continuous scaling of semiconductor devices, the formation of diffusion barrier layers has changed, especially for TiN, which is widely used in the fabrication process. Among various deposition methods, atomic layer deposition (ALD) has been actively investigated because of its atomic-scale thickness controllability and excellent step coverage. Typically, thermal ALD uses a thermal energy source to induce chemical reactions to deposit TiN thin films. For ALD TiN research, studies have been conducted in the process temperature range of 200–500 °C. However, a high electrical resistivity, high concentration of impurities, and low failure temperature for Cu diffusion were observed even in this temperature range. Consequently, plasma-enhanced ALD (PEALD), which simultaneously supplies heat and plasma energy, has been gaining attention for producing high-quality TiN thin films.[13–17]

Hollow cathode plasma (HCP) has recently attracted considerable attention as a new plasma source for PEALD. Unlike conventional plasma sources, such as capacitively coupled plasma (CCP), inductively coupled plasma (ICP), and microwave plasma (MP), HCP has the advantage of preventing oxygen contamination due to the etching of the dielectric liner inside the equipment, which is

considered an important process factor that determines the film properties during nitride and non-oxide film deposition. HCP forms plasma using the same principle as conventional CCP; however, the difference lies in the direction and density of the radicals formed in the plasma. Holes exist in the cathode structure; ions and electrons are trapped in the holes, resonate inside the walls of the cavity, collide with the injected gas species, and form plasma. Simultaneously, a high electron density and plasma with a density 2–3 times higher than that of CCP can be obtained owing to the hole, which is called the hollow cathode effect.[17] Because the entire part generating plasma comprises metal (stainless steel), oxygen contamination owing to the presence of dielectrics in the plasma generator, such as ICP and MP, can be neglected, facilitating the deposition of non-oxide thin films, such as metals and their nitrides. Finally, the number of ion species that accelerated directly onto the substrate was small, which resulted in low plasma damage and excellent growth rates. Because of these advantages, HCP is attracting attention as a new plasma source to replace other plasma sources, and deposition research on nitride materials, such as AlN, AlGaN, InN, and SiN, is being actively conducted.[1,4,17–23]

In this study, HCP-assisted ALD (HCP-ALD) was used to fabricate high-quality TiN thin films with copper diffusion barriers. During this process, the deposition temperature range was set to 200–300 °C. Moreover, the structural, chemical, and electrical properties of the films within the low-temperature range were analyzed to compare and understand the film properties according to the deposition temperature. Furthermore, the step coverage and Cu diffusion barrier characteristics of TiN thin films, which could be the primary concerns for diffusion barrier applications, were evaluated.

II. EXPERIMENT

A schematic diagram of the HCP-ALD instrument used in this study is shown in Fig. 1(a). The PEALD instrument was modified using a traveling-wave-type thermal ALD instrument (Atomic Classic, CN-1, Korea). The HCP was Series 50 from Meaglow (Canada), which can apply up to 600 W of DC and RF power. Figure 1(b) shows a schematic of the TiN deposition process using HCP-ALD. $TiCl_4$ was used as the Ti precursor, NH_3 plasma was used as the reactive gas, and N_2 was used as the purge and carrier gas for TiN deposition. The process sequence was $TiCl_4$ injection (1 s), N_2 purge (60 s), NH_3 plasma pulse (15 s), N_2 purge (60 s), and one ALD cycle that comprises these four gas pulses. The process temperatures were mainly 200, 230, 250, 280, and 300 °C, and the plasma power was set to 300 W, which was optimized to obtain low film resistivity. The thickness of the deposited TiN was measured using the Drude-Lorentz mode of an ellipsometer (Film Sense, FS-1, USA) and verified using cross-sectional scanning electron microscopy.

TiN thin films deposited through HCP-ALD were characterized using x-ray diffraction (XRD, Rigaku, Dmax 2500, Japan), x-ray fluorescence (XRF, ARL, QUANTX, USA), x-ray reflectometry (XRR, Rigaku, Smart Lab, Japan), focused ion beam (Crossbeam, Germany), transmission electron microscope (Cs-TEM, JEOL, NEO ARM, Japan), atomic force microscope (AFM, Park, XE-7, Korea), and 4-point probe (AIT, CMT-100, Korea) to analyze the physical
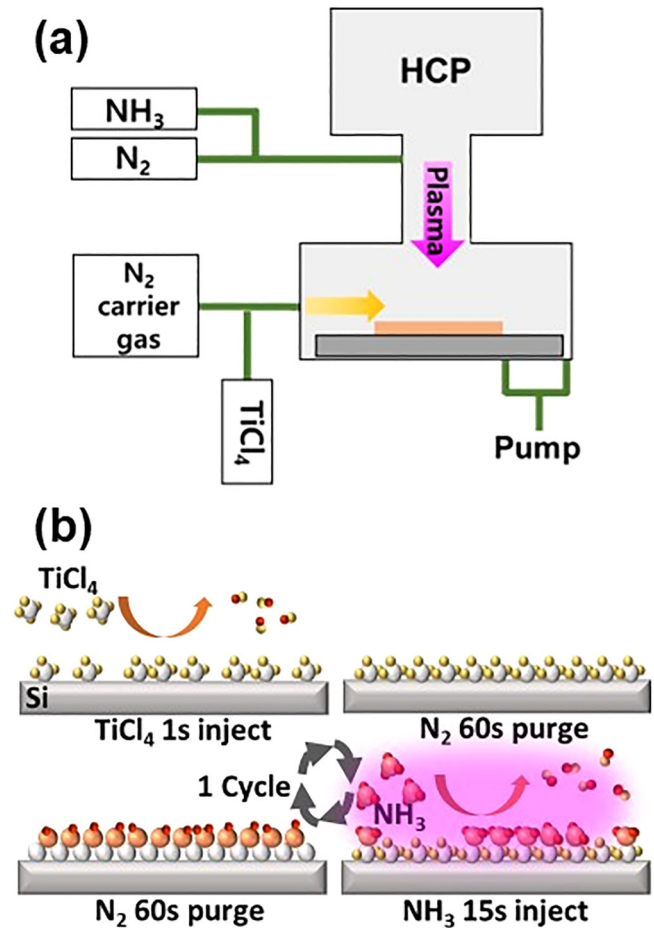

FIG. 1. (a) Schematic of HCP-ALD apparatus, (b) schematic of HCP-ALD process of the TiN film.

properties of TiN thin films. Auger electron spectroscopy (AES, Physical Electronics, PHI-710, USA), x-ray photoelectron spectroscopy (XPS, Physical Electronics, PHI-5000 Nexa, USA), Rutherford back-scattering spectroscopy (RBS, NEC, Japan), and time-of-flight secondary ion mass spectroscopy (ToF-SIMS, Spectral, ToF SIMS 5, Sweden) were used to characterize the chemical properties of TiN thin films.

Rapid thermal annealing (RTA, Ultech, Real RTP-100, Korea) was used to conduct copper diffusion experiments. The copper diffusion test was performed by depositing 100 nm of Cu on a TiN thin film grown on SiO_2 and Si substrates and subjecting it to 30 min of RTA at 200, 400, 600, 700, and 800 °C in a vacuum atmosphere.

III. RESULTS AND DISCUSSION

A. Growth of a TiN film

The ALD process varies with the film growth rate depending on the deposition temperature, time at which the precursor and

reaction gases are injected, and purge time. Therefore, the ALD process conditions were explored by observing the changes in the growth rate. Figures 2(a) and 2(c) show the areal density of Ti as a function of the $TiCl_4$ feeding time, NH_3 plasma feeding time, and purging time at a 300 °C process temperature. The areal density of Ti was measured using XRF after thin-film deposition on a Si substrate. Figure 2(a) shows that the Ti areal density increased with increasing injection time and became constant after 1 s. For NH_3 plasma application times in the range of 20–30 s, a continuous increase in film density with increasing pulse time was observed, as shown in Fig. 2(b). The ideal ALD film growth behavior converged to a certain level with increasing application time, such as the Ti precursor injection time, which was not confirmed in the experiments on the NH_3 plasma time. Tiznado and Zaera reported that additional TiN growth could occur during NH_3 treatment owing to the reaction of re-desorbed $TiCl_4$ from the walls of the reactor, which resulted in unstable growth reproducibility.[24] In our case, a high Ti areal density was reproducibly obtained after 15 s of plasma treatment. Therefore, a 15 s application condition was set as the process condition. In the case of $TiCl_4$ purged with N_2 gas, as the purge time increased, the areal density of Ti decreased sharply and then converged to a constant value, with the converged value starting at 30 s. However, we set the $TiCl_4$ purge time to 60 s because a long purge time could minimize the equipment damage due to

residual Cl-related gas molecules. For after purging NH_3, the areal density of Ti decreased at 60 s. Therefore, based on these results, the process time conditions were set as $TiCl_4$ injection (1 s), N_2 purge (60 s), NH_3 plasma pulse (15 s), and N_2 purge (60 s) for the deposition experiment.

The growth per cycle (GPC, same as the growth rate) of TiN in the temperature range of 170–350 °C is calculated to compare the TiN thin film properties with respect to the deposition temperature, and the results are shown in Fig. 2(d). The process temperature was subdivided into 170, 200, 230, 250, 280, 300, 330, and 350 °C within the mentioned temperature range, and the thickness of the film was measured using an ellipsometer according to the number of ALD cycle. Figure 2(d) shows a constant GPC of approximately 0.5 Å/cycle in the temperature range of 170–300 °C, indicating that this temperature range represents the ALD window for the ALD process. GPC was largely increased above 300 °C, which could be attributed to the increased adsorption and reaction of gas molecules. Although the experiments for the process time conditions were performed based on a process temperature of 300 °C, similar GPC was observed over the temperature range of the ALD window. Therefore, the process-time conditions can be readily applied in this temperature range. The GPC was similar in the ALD window; however, the properties of the TiN films differed owing to the temperature effect.
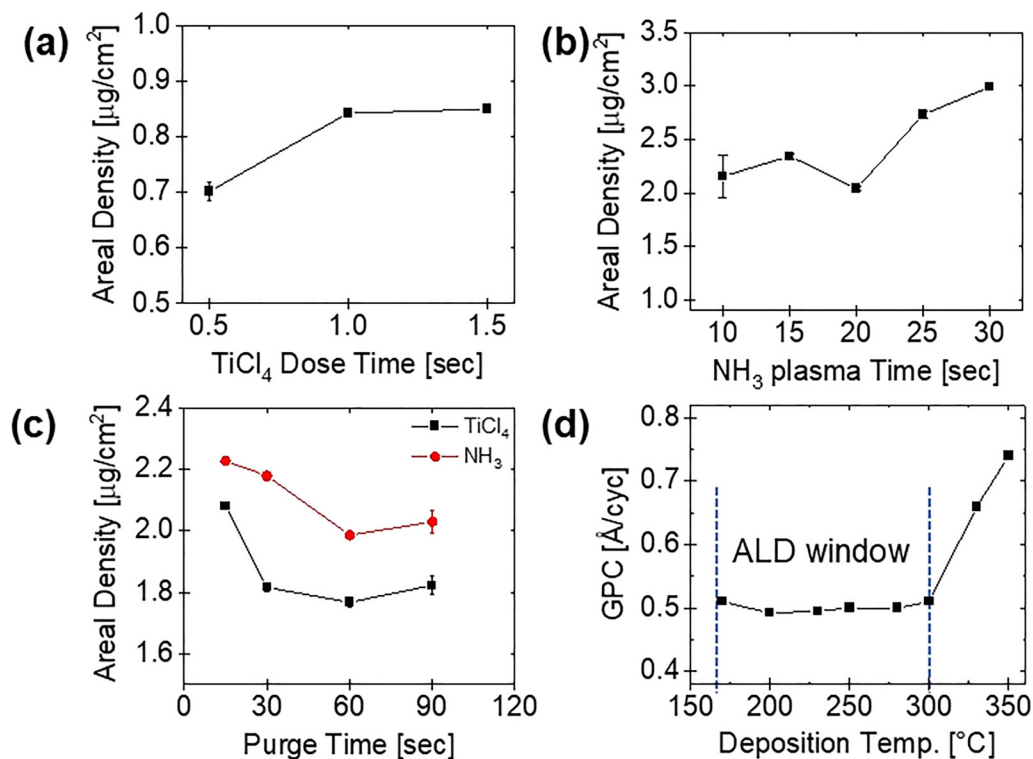
FIG. 2. Variation in Ti areal density (a) according to $TiCl_4$ dose time, (b) NH_3 plasma pulse time, (c) $TiCl_4$ and NH_3 purging time, and (d) GPC of the TiN film depending on deposition temperature.

B. Structural and physical properties of the TiN film

Figure 3 shows the XRD patterns of TiN thin films as a function of the deposition temperature. Regardless of the temperature, it has an FCC polycrystalline structure, with (200) as the primary peak and (111) as the emerging peak. The intensity of all the peaks increased, and the width of the peak decreased with increasing process temperature. Consequently, it is predicted that the crystallinity of the TiN film increases with increasing process temperature and that the grain size increases owing to the growth of crystallites in the film. The diffraction peak intensity increased with increasing deposition temperature, and the size of the grains obtained from the Scherrer method increased by approximately 2 times at 300 °C compared to that at 200 °C for the (111) plane. Average grain sizes of (111) were 4.19, 4.81, 5.58, 9.10, and 10.21 nm at 200, 230, 250, 280, and 300 °C, respectively. Note that the peak intensity of the (111) plane was significantly increased in the film grown at 280 °C. Differences in crystallographic properties, such as crystallinity and grain size, attributed to grain growth at increasing process temperatures eventually affect the electrical properties of TiN.[25–29]

Figure S1 (Ref. 48) shows the XRR analysis results for the 25 nm thick TiN thin film at different deposition temperatures. The thickness, roughness, and density of the TiN films were determined using XRR analysis. The thickness of the film showed an error of approximately 5% from ellipsometer measurements, and the surface roughness was approximately 1 nm higher than that obtained using AFM. The density of the deposited TiN thin film is summarized by comparing the theoretical bulk density (5.44 g/cm^3) with the sputter-deposited 100 nm thick TiN (5.05 g/cm^3), as shown in Fig. 4.[6,30] In the 200–300 °C deposition temperature range, the density exhibited a thin film density of 5.07–5.29 g/cm^3. As the deposition temperature increased, the film density increased and a similar density of 5.2 g/cm^3, on average, was observed in the intermediate temperature range of 230–280 °C. The densest film of
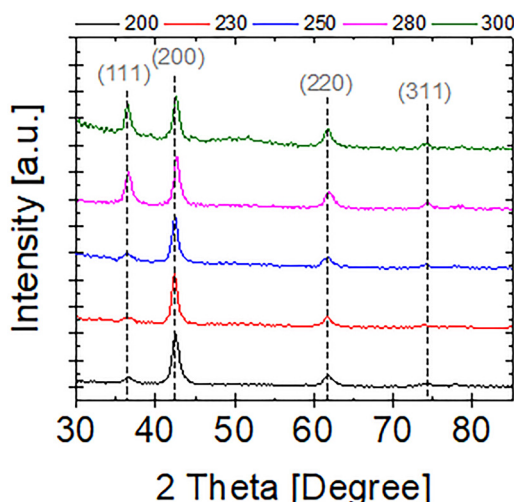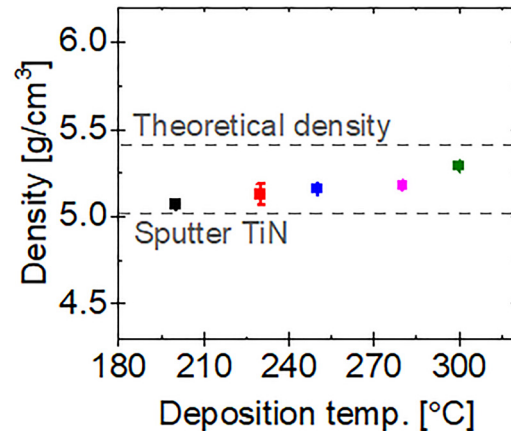

FIG. 4. Variation in the density of TiN films as a function of deposition temperature from x-ray reflectometry.

5.29 g/cm^3 is formed at 300 °C, which was attributed to the increased crystallinity of the film and the growth of the (111) facets, which is the densest facet, as confirmed by the XRD results. The highest film densities were obtained for the TiN thin films, indicating that the HCP-ALD process is capable of forming dense films with a density of approximately 98% of the bulk density.[25,29,31–34] As the TiN film density increased, the electrical resistivity and diffusion barrier properties improved.

Figures 5(a)–5(d) show the AFM results and root-mean-square roughness (R_{rms}) of the as-deposited TiN thin films as a function of deposition temperature. The R_{rms} values extracted from the AFM analysis of 25 nm thick TiN thin films deposited at 200, 230, 250, 280, and 300 °C are shown in Fig. 5(d). The R_{rms} decreased by approximately 24% from ~1.5 nm at 200 °C to ~1.14 nm at 300 °C with increasing deposition temperature. Usually, grain growth during post-deposition annealing makes the film rougher owing to the different grain growth rates along the crystallographic direction. However, the coexistence of dense (111) and (200) planes likely produced a smoother surface at elevated temperatures. Cross-sectional TEM images of the TiN film grown at 300 °C exhibited the uniform film formation and columnar structures of the (111) and (200) planes, as shown in Figure S2.[48] The decrease in R_{rms} of the thin film also affected the decrease in the electrical resistivity of the thin film, which will be discussed later when the electrical properties are explained.

C. Chemical properties of the TiN film

Figure 6 shows the results of analyzing the chemical state in the thin film through AES depth profile analysis of TiN films. The results for the 200–300 °C process conditions are shown in Figs. 6(a)–6(e), and the averaged atomic-level concentrations of the constituent elements are summarized in Fig. 6(f). Here, film thickness ranged from 20 to 30 nm, and different sputtering power conditions were applied for each analysis. Accurate elemental separation becomes difficult because of the overlap of the Auger electron energies of Ti and N in the AES depth profile; therefore,

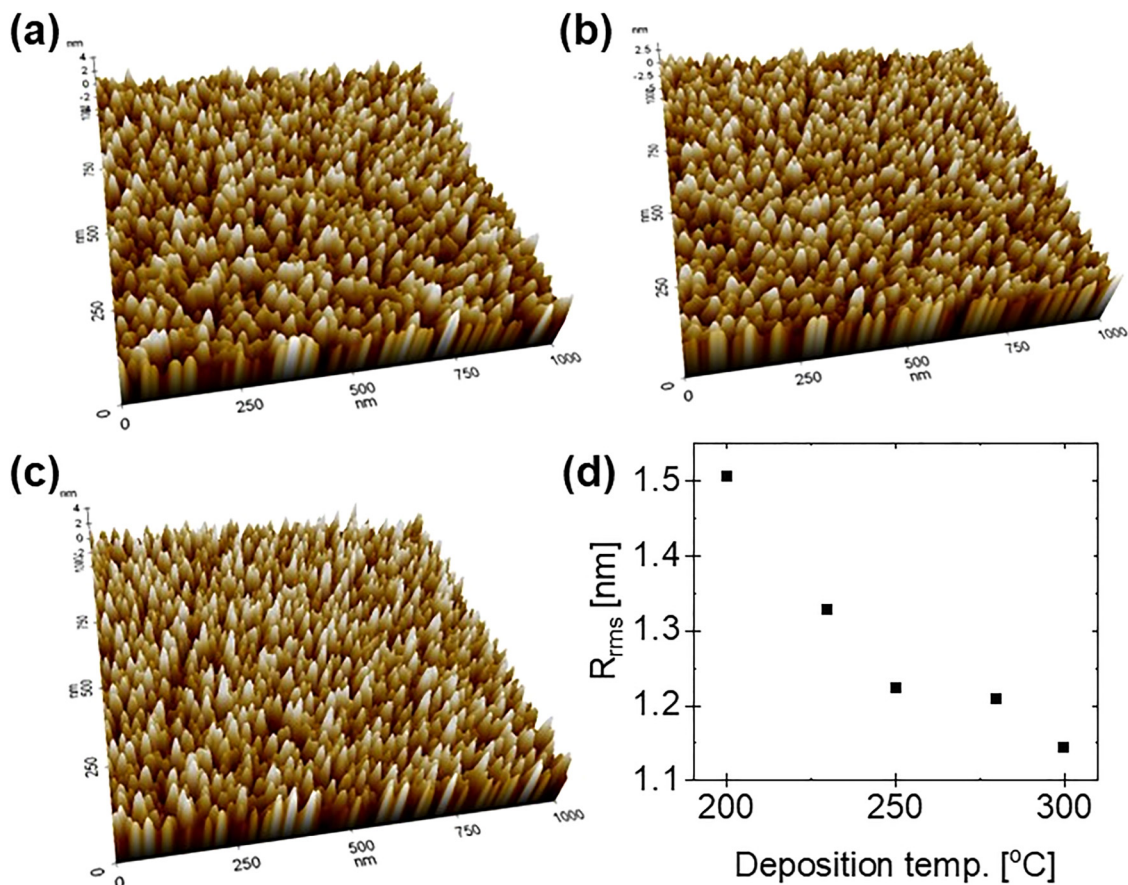FIG. 3. X-ray diffraction patterns of TiN films as a function of deposition temperature.

FIG. 5. Atomic force microscope images of TiN films grown at (a) 200, (b) 250, (c) 300 °C, and (d) R_{rms} depending on deposition temperature.

for accurate film composition analysis, RBS analysis was subsequently performed. Moreover, the depth profiles of Ti and N+Ti in the TiN films were similar regardless of the process conditions, whereas C was present in 0.2–1 at. %, O in 1.5–2.87 at. %, and Cl in 0.004–0.12 at. %. The lower amounts of C and O were attributed to the HCP-ALD process, which facilitated the deposition of nitride and non-oxide thin films. Low content of C and O could have originated from the processing gas, substrate, and air exposure. In particular, the small amount of Cl is attributed to the sufficient ligand exchange at 200–300 °C during the HCP-ALD process, which results in a high plasma density.[25,32] Minor presence of Cl is attributed to the re-adsorption of HCl byproducts.[24] This obtained state is a very low impurity concentration compared with ICP-ALD TiN in Table S1,[48] and the impurity concentration is expected to be influenced more by the plasma generation device and plasma process variables, such as plasma power and exposure time, which affect the ion and radical conditions during the process, than by the process temperature.[10–12,15–21,25,32,33,35–39] ICP-ALD grown TiN films had 0.5–1.9 at. % Cl in the films.[29,31,35,39] Table S1 (Ref. 48) shows that our TiN films had very low Cl impurity levels compared to those from TiN films grown by ICP-ALD. The concentration of

Cl among the impurities tended to decrease with increasing deposition temperature, which was further analyzed using ToF-SIMS.

The concentration of impurities detected by the AES depth profile was confirmed; however, a more precise comparison was made using ToF-SIMS analysis, which had better sensitivity than the AES depth profile. Figure 7 shows the ToF-SIMS analysis results for the HCP-ALD TiN thin films deposited at 200, 250, and 300 °C, demonstrating the differences in the amounts of C, O, and Cl impurities depending on the deposition temperature. The intensity of C remained constant at approximately 250–300 counts under all temperature conditions; therefore, the amount of C was independent of the deposition temperature. Next, the intensity of O gradually decreased in the order of approximately 17 500, 12 500, and 8500 counts, as shown in Figs. 7(a)–7(c), respectively. The intensity of Cl also decreased as the process temperature increased, in the order of approximately 12 000, 7000, and 2500. The decreasing tendency of Cl is attributed to the active occurrence of ligand exchange reactions for film deposition as the deposition temperature of the film increased, which reduced the amount of residual impurities in the film and improved the film properties such as electrical resistivity and film density.
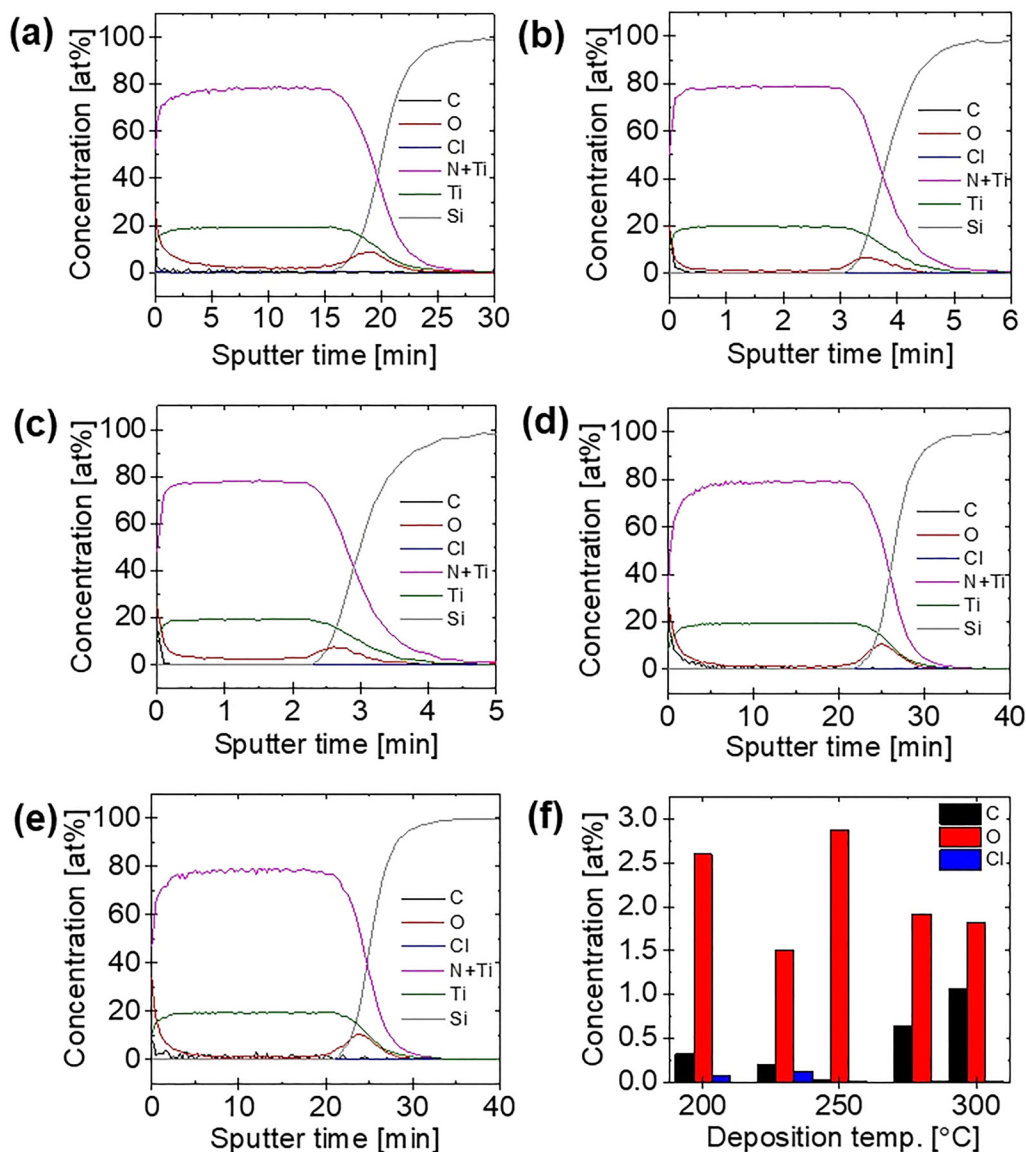
FIG. 6. Auger electron spectroscopy depth profiles of TiN films grown at (a) 200, (b) 230, (c) 250, (d) 280, (e) 300 °C, and (f) averaged atomic concentration of C, O, and Cl.

Figure 8 shows the XPS spectra of Ti 2p, N 1s, and O 1s in the TiN thin films as a function of process temperature, indicating the bonding state of TiN. Figures 8(a)–8(c) show the Ti 2p spectra of TiN films grown at 200, 250, and 300 °C. Regardless of the process temperature, Ti 2$p_{3/2}$ was in the range of 455–460 eV and Ti 2$p_{1/2}$ was in the range of 460–465 eV. Peak deconvolution revealed that the TiN film was composed of Ti–N, Ti–O–N and the satellite peaks of TiN. The primary Ti-N subpeak exhibits a binding energy of 455 ± 0.5 eV and appears in the range of 455.0–455.2 eV.[13,32,40–43] Ti–O–N has a binding energy range of 456.2 ± 0.4 eV and appears in the range of 456.1–456.3 eV.[29,37,44–47]

Ti–O–N is attributed to oxidation from the surface through the grain boundaries. The satellite peak was observed in the range of 457.2 ± 0.6 eV and appeared at 457.5–457.9 eV.[13,32,40–43] The satellite peak of TiN corresponds to stoichiometric TiN$_x$ with $x > 0.8$.[40] Ti–O bonding should have evolved in the range of 458.4–459 eV due to oxidation, but it was masked by the satellite peak of TiN.

Figures 8(d)–8(f) show the N 1s XPS spectra of TiN films grown at 200, 250, and 300 °C. Peak deconvolution revealed that the TiN film was composed primarily of Ti–N bonds with minimal amounts of Ti–O–N and TiN satellite peaks, consistent with Ti 2p. The peak position shifted to a higher binding energy with an
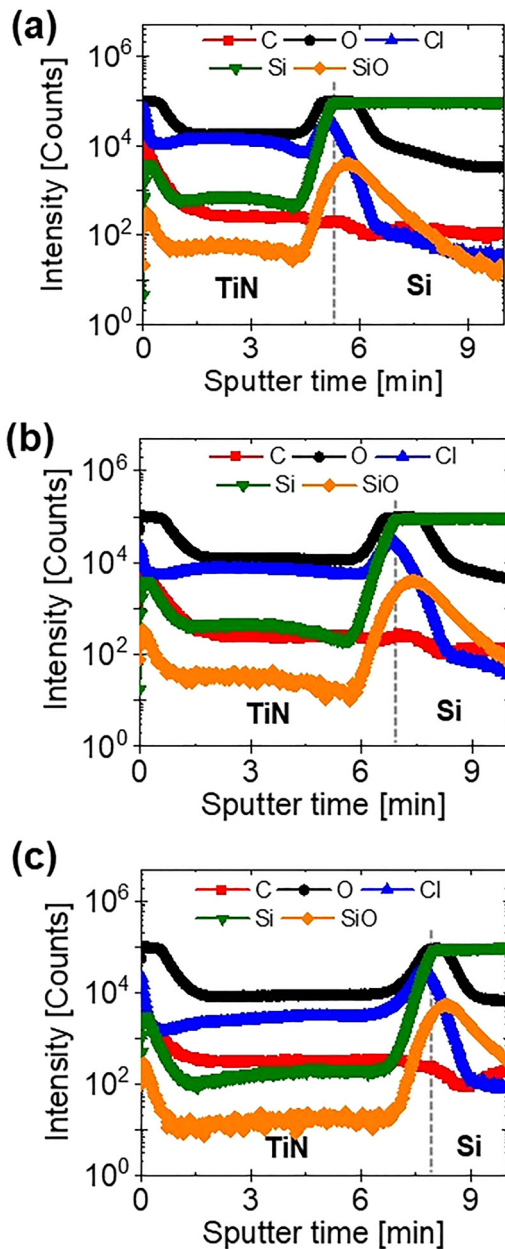
FIG. 7. Elemental depth profile of time-of-flight secondary ion mass spectroscopy analysis on TiN films grown at (a) 200, (b) 250, and (c) 300 °C.

increase in the deposition temperature, indicating that stronger bonds were formed at elevated temperatures. Figures 8(g)–8(i) show the O 1s XPS spectra, where the subpeaks from Ti–O, Ti–O–N, and absorbed OH are indicated by peak deconvolution. As mentioned previously, the surface and grain boundaries of TiN could be the primary sources of oxygen-related species. *In situ* XPS analysis of the as-grown TiN film is required in this regard. XPS analysis of TiN thin films grown at various temperatures showed that the film existed primarily in the Ti–N state, regardless of the temperature, and it can be predicted that a near-stoichiometric TiN thin film was formed based on the occurrence of satellite peaks.

RBS analysis was performed on the TiN specimens deposited at 300 °C, as there was no significant deviation in the process temperature and chemical composition during the AES and XPS analyses. Although it was difficult to determine the exact composition ratio of Ti and N in the AES depth profile, observation of the satellite peak during XPS analysis predicted that the deposited film was near-stoichiometric TiN_x with $x > 0.8$. In the RBS analysis, the Ti:N ratio was confirmed to be 1:0.95, as shown in Figure S3,[48] indicating that a $TiN_{0.95}$ thin film was deposited, which is very close to the stoichiometric ratio.

D. Electrical properties, step coverage, and Cu diffusion barrier characteristics

One of the primary factors affecting the electrical resistivity of thin films is the mean free path of electrons, which is related to grain boundaries and surface scattering. In addition, impurities in thin films can act as electron-scattering elements. The density of the film was related to its electrical resistivity; as the density increased, the electrical resistivity inversely decreased. This is likely because scattering factors, such as voids and impurities in the film, decrease as the film density increases.[25–27,31–33,35,44]

Figure 9 shows the electrical resistivity of TiN thin films deposited using HCP-ALD as a function of the deposition temperature and film thickness. The electrical resistivity decreased with increasing deposition temperature and film thickness, with the lowest electrical resistivity of 132 $\mu\Omega$ cm observed for the 35 nm thick film deposited at 300 °C. A resistivity of 200 $\mu\Omega$ cm has been reported for a 100 nm thick TiN film deposited by sputtering and a 32 nm thick TiN film grown at 400 °C using ICP-ALD. A similar or lower electrical resistivity was observed for the 35 nm TiN thin film, regardless of the deposition temperature. Therefore, HCP-ALD of TiN can achieve excellent electrical resistivity properties at lower temperatures and thinner thicknesses than other processes.

The effect of the process temperature on the electrical resistivity can be explained by grain growth and impurity concentration. As the processing temperature increased, the electrical resistivity decreased, which was likely attributed to the increase in the grain size and decrease in the surface roughness of the polycrystalline TiN thin films. Consequently, as the process temperature increases, the degree of grain boundary scattering and surface scattering of electrons decreases, resulting in an improvement in the electrical resistivity characteristics. In addition, the film density increased as the process temperature increased, and the electrical resistivity decreased because of an improved density. A correlation was observed between the impurity concentration and electrical resistivity; the decrease in the amount of residual Cl with increasing process temperature, as confirmed by AES and ToF-SIMS, contributed to the decrease in electrical resistivity.

Next, a trench pattern with a width of 80 nm and a height of 2.5 μm with an aspect ratio of 32:1 (Fig. S4)[48] was used for the step covering test in the HCP-ALD of TiN. The step coverage test was performed at 200, 250, and 300 °C. Figures 10(a)–10(c) show the sidewall and bottom step coverages observed using HR-SEM. It was
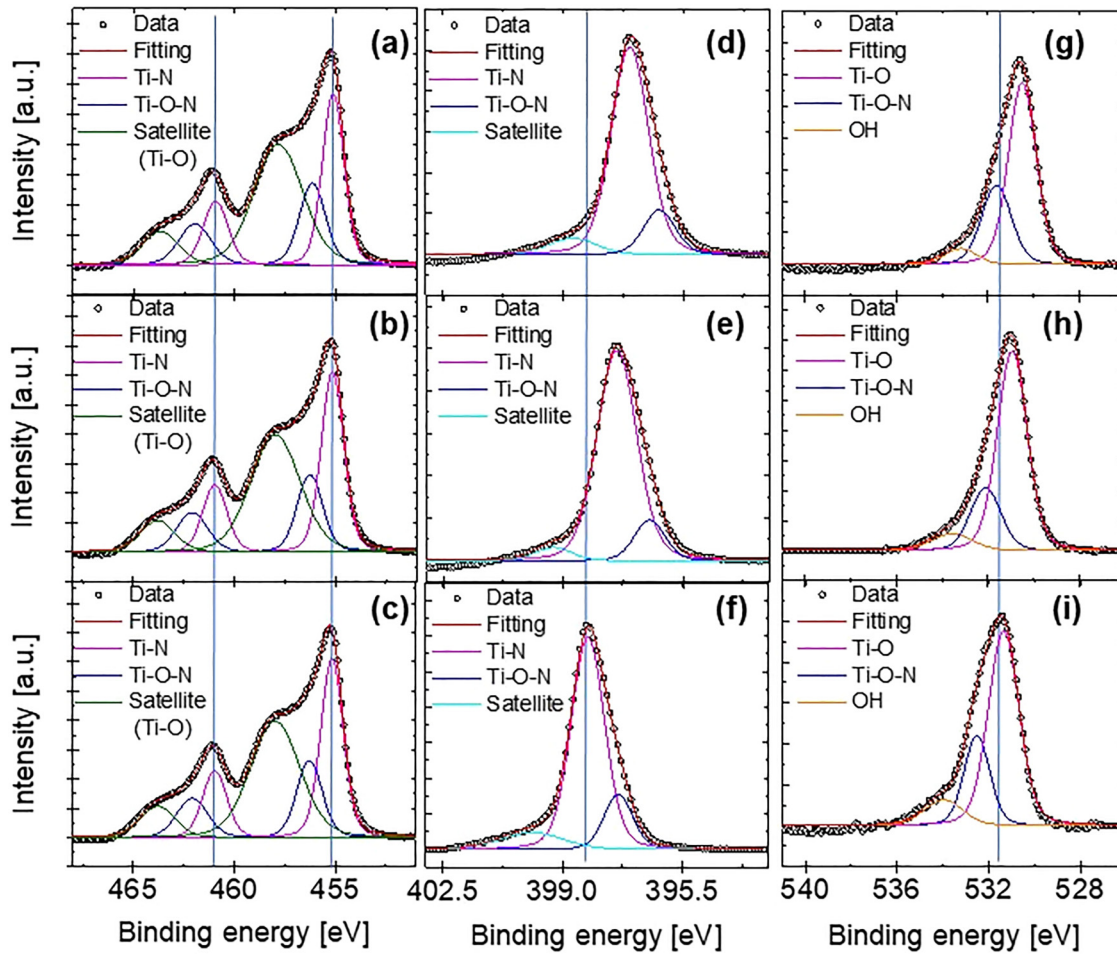
FIG. 8. X-ray photoelectron spectroscopy spectra of TiN films deposited at 200, 250, and 300 °C, respectively. (a)–(c) Ti 2p, (d)–(f) N 1s, and (g)–(i) O 1s.

observed that the sidewall step coverage was 100% and the bottom step coverage was 99% for the 200 °C process, whereas the sidewall and bottom step coverages deposited at 250/300 °C were 100%/99% and 100%/98%, respectively. This excellent step coverage indicates that the HCP-ALD TiN process enables the formation of uniform thin films on nanostructures with high aspect ratios.

Typically, the PEALD process is known to have poor step-coverage characteristics compared to thermal ALD processes because recombination-limited growth behavior was observed in the PEALD process. Recombination-limited growth behavior implies that reactant gases in the plasma impinge on the surface and react with surface-adsorbed atoms and molecules, which are removed and no longer contribute to the film growth. In particular, the step coverage of the metallic thin films is lower because of the higher probability of recombination on the metallic surface. Excellent step coverage characteristics were obtained at an aspect ratio of 32:1. To improve the step coverage property of the PEALD process, a high density of radicals is injected to negate the recombination process, forming a

larger radical flux that can reach the depth direction of the trench with a large aspect ratio and enhance the step-coverage property of the deposited thin film. Because HCP is a plasma generator that utilizes the hollow cathode effect to form a higher plasma density than conventional plasma generators, it was predicted that HCP-ALD TiN would have excellent step coverage characteristics. In addition, in the process temperature range of 200–300 °C, all of them show excellent step coverage characteristics, and thus, the step coverage is not affected by temperature.

Finally, the Cu diffusion barrier properties of the HCP-ALD TiN thin films were evaluated using TiN thin films deposited at 300 °C, which have high density and low electrical resistivity, and are thus expected to have excellent Cu diffusion barrier properties. Specimens for the Cu diffusion test were fabricated by depositing approximately 10, 15, and 22 nm of HCP-ALD TiN on Si and SiO$_2$ substrates at 300 °C, and depositing 100 nm of Cu by sputtering on them. The specimens were subjected to vacuum RTA at 200, 400, 600, 700, and 800 °C for 30 min. Subsequently, the specimens on
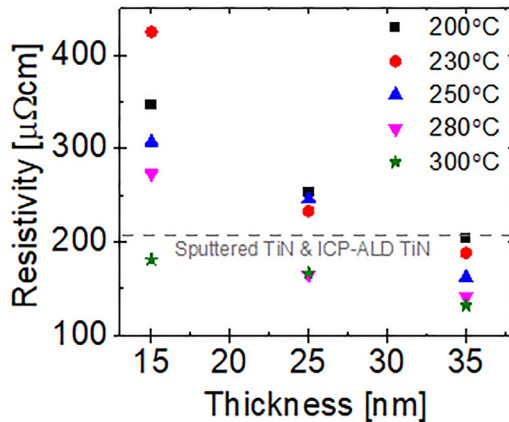
FIG. 9. Resistivity of TiN films according to the deposition temperature and film thickness.

the SiO_2 substrates were used for sheet resistance measurements, whereas those on the Si substrates were used for XRD and SEM analyses. Figure 11(a) shows the sheet resistance of the specimens as a function of RTA temperature and TiN thickness. All of the HCP-ALD grown TiN films showed a sharp increase in sheet resistance after RTA at 700 °C, which can be attributed to the diffusion of Cu atoms into the SiO_2 or Si layer underneath, and the formation of Cu_3Si with low conductivity, such that the Cu layer becomes discontinuous and exhibits a higher resistance. Therefore, the thin film of 10–22 nm thick TiN retains its anti-copper diffusion property up to 600 °C. The formation of Cu_3Si was confirmed using XRD, as shown in Fig. 11(b). After the RTA at 600 °C, the XRD pattern shows a crystalline peak of TiN, which can act as a Cu diffusion barrier up to 600 °C. After RTA at 700 °C, the intensity of the TiN phase decreased, but the Cu_3Si phase emerged. After RTA at 800 °C, the TiN phase almost completely disappeared owing to the Cu diffusion.

The film thickness, density, and grain size are known to influence the properties of the Cu diffusion barrier. TiN thin films grown using ICP-ALD were found to have failure temperatures of 617 °C for 5 nm and 600 °C for 31.8 nm.[28,38] However, the anti-diffusion property of the 5 nm thick film was evaluated at 617 °C for only 2 s; therefore, it was difficult to directly compare it with the 10 nm thick TiN film grown by HCP-ALD with the Cu anti-diffusion property at 600 °C for 30 min. Therefore, the 10.3 nm thick TiN film grown by HCP-ALD exhibited the same Cu diffusion barrier properties as the 32 nm thick film grown by ICP-ALD at the same temperature and time.[27,29,33,36–38]
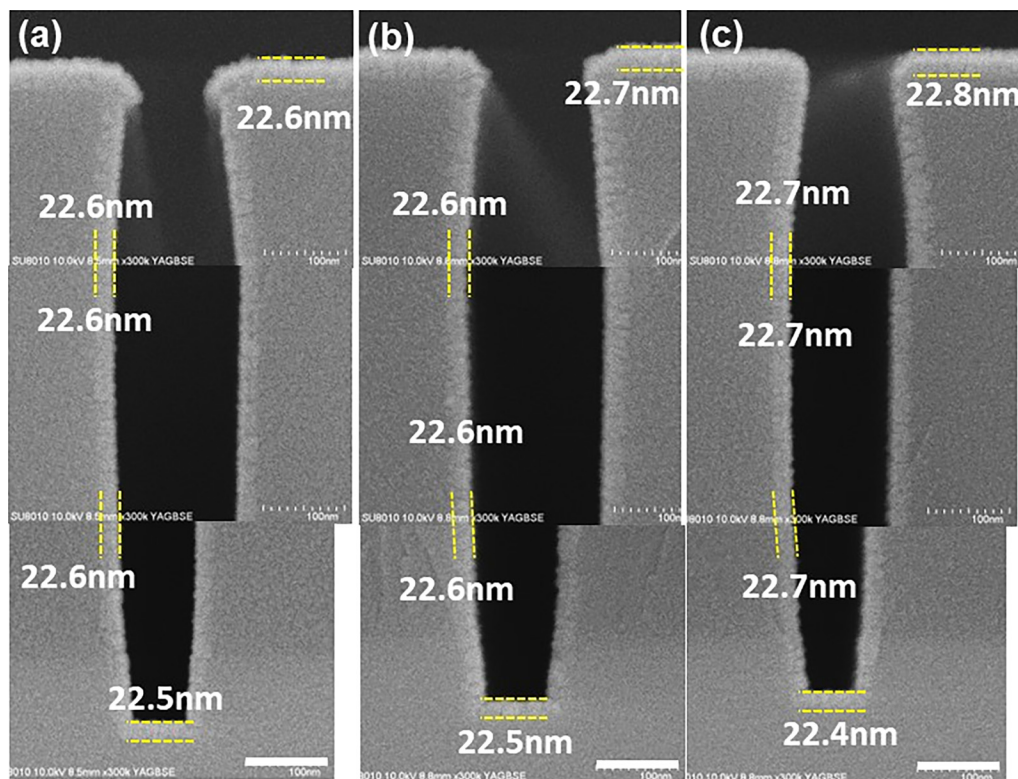

FIG. 10. Cross-sectional transmission electron microscopy images of trench pattern with a 32:1 aspect ratio for TiN films deposited at (a) 200, (b) 250, and (c) 300 °C (scale bar: 100 nm).
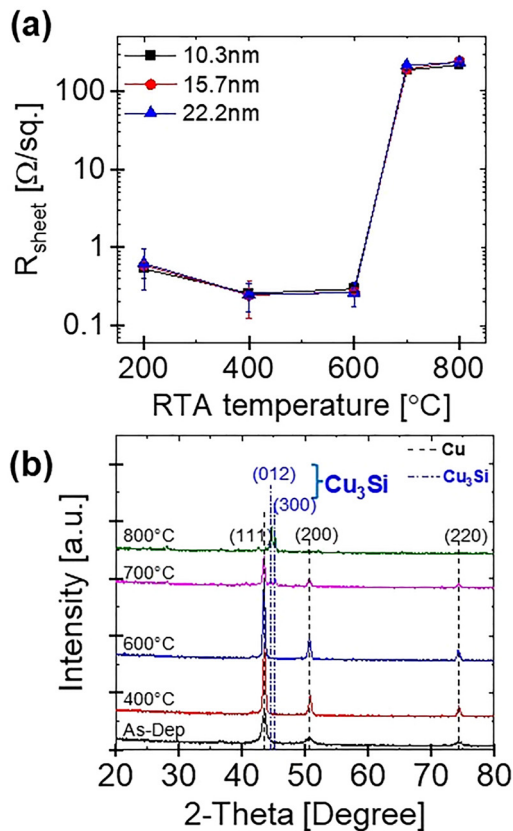
(a)

(b)

FIG. 11. (a) Variation in sheet resistance and (b) XRD patterns depending on RTA temperature for Cu diffusion barrier characteristics.

IV. SUMMARY AND CONCLUSIONS

In this study, we investigated the properties of TiN thin films deposited in the temperature range 200–300 °C using a novel plasma source, the HCP-based ALD process. The effect of the deposition temperature on the film properties was analyzed by evaluating the crystallographic, physical, chemical, and electrical properties of TiN films. The TiN thin film was polycrystalline with an FCC crystal structure, and the intensity of the (111) peak, which is the densest plane, increased with increasing deposition temperature, consequently increasing the grain size. A near-stoichiometric composition of $TiN_{0.95}$ was formed with low variation in Ti and N concentrations. Very low impurity concentrations of C 0.32–1%, O 1.5–2.9%, and Cl 0.004–0.12% were found. These differences as a function of the deposition temperature affected the film density and electrical resistivity. As the deposition temperature increased, the film density increased and the electrical resistivity decreased. It was observed that a dense thin film was formed with a value similar to the bulk density of 5.29 g/cm^3 at 300 °C, and the electrical resistivity was found to be 132 $\mu\Omega$ cm in the 32 nm thick film deposited at 300 °C. High-quality TiN copper anti-diffusion films with high density and excellent step coverage were fabricated using an HCP-based PEALD process. This study explains a new method for fabricating TiN films, which is helpful for the application of high-quality TiN films as Cu diffusion barriers.

AUTHOR DECLARATIONS

Conflict of Interest

The authors have no conflicts to disclose.

Author Contributions

Ha Young Lee: Conceptualization (equal); Data curation (equal); Formal analysis (equal); Investigation (equal); Methodology (equal); Visualization (equal); Writing – original draft (lead); Writing – review & editing (equal). **Jeong Hwan Han:** Conceptualization (equal); Investigation (equal); Writing – original draft (supporting); Writing – review & editing (supporting). **Byung Joon Choi:** Conceptualization (equal); Data curation (equal); Formal analysis (equal); Investigation (equal); Supervision (lead); Visualization (equal); Writing – original draft (supporting); Writing – review & editing (lead).

DATA AVAILABILITY

The data that support the findings of this study are available from the corresponding author upon reasonable request.

REFERENCES

[1] M. Y. Kwak, D. H. Shin, T. W. Kang, and K. N. Kim, Thin Solid Films **339**, 290 (1999).

[2] T. Oku, E. Kawakami, M. Uekubo, K. Takahiro, S. Yamaguchi, and M. Murakami, Appl. Surf. Sci. **99**, 265 (1996).

[3] F. Battegay and F. Hodaj, J. Mater. Sci. Mater. Electron. **27**, 1679 (2016).

[4] H. C. Chen, B. H. Tseng, M. P. Houng, and Y. H. Wang, Thin Solid Films **445**, 112 (2003).

[5] J. Uhm and H. Jeon, Jpn. J. Appl. Phys. **40**, 4657 (2001).

[6] M. Moriyama, T. Kawazoe, M. Tanaka, and M. Murakami, Thin Solid Films **416**, 136 (2002).

[7] S.-H. Kwon, O.-K. Kwon, J.-S. Min, and S.-W. Kang, J. Electrochem. Soc. **153**, G578 (2006).

[8] A. Gupta, H. Wang, A. Kvit, G. Duscher, and J. Naraya, J. Appl. Phys. **93**, 5210 (2003).

[9] S. Lee Y, J. Mack, H. Y. Kim, S.-H. Jung, S. J. Rathi, and N. Mukherjee, Mater. Lett. **315**, 131912 (2022).

[10] H. Kim, C. Cabral, Jr., C. Lavoie, and S. M. Rossnagel, J. Vac. Sci. Technol. B. **20**, 1321 (2002).

[11] E. Kolawa, J. S. Chen, J. S. Reid, P. J. Pokela, and M. A. Nicolet, J. Appl. Phys. **70**, 1369 (1991).

[12] H. Ono, T. Nakano, and T. Ohta, Appl. Phys. Lett. **64**, 1511 (1994).

[13] B. S. Suh, Y. J. Lee, J. S. Hwang, and C. O. Park, Thin Solid Films **48**, 299 (1999).

19 March 2024 01:10:25

[14]C. L. Lin, P. S. Chen, C. L. Chang, and M. C. Chen, J. Vac. Sci. Technol. B 20, 1947 (2002).

[15]S. M. George, Chem. Rev. 110, 111 (2010).

[16]W. Zhang, S. H. Brongersma, O. Richard, B. Brijs, R. Palmans, L. Froyen, and K. Maex, Microelectron. Eng. 76, 146 (2004).

[17]Y. J. Lee, H. W. Yeon, S. Y. Jung, S. K. Na, J. S. Park, Y. Y. Choi, H. J. Lee, O. S. Song, and Y. C. Joo, Electron. Mater. Lett. 10, 275 (2014).

[18]H. Wang, J. Li, K. Li, Y. P. Lin, J. Chen, L. J. Gao, V. Nicolosi, X. Xiao, and J. M. Lee, Chem. Soc. Rev. 50, 1354 (2021).

[19]S. Q. Wang, I. Raaijmakers, B. J. Burrow, S. Suthar, S. Redkar, and K. B. Kim, J. Appl. Phys. 6, 5176 (1990).

[20]V. Lingwal and N. S. Panwar, J. Appl. Phys. 97, 104902 (2005).

[21]K. C. Park, K. B. Kim, I. J. M. Raaijmakers, and K. Ngan, J. Appl. Phys. 80, 5674 (1996).

[22]R. Leutenecker, B. Frijschle, U. Cao-Minh, and P. Ramm, Thin Solid Films 270, 621 (1995).

[23]L. Djomeni et al., Microelectron. Eng. 120, 127 (2014).

[24]H. Tiznado and F. Zaera, J. Phys. Chem. B 110, 13491 (2006).

[25]Y. H. Shin and Y. Shimogaki, Sci. Technol. Adv. Mater. 5, 399 (2004).

[26]C. S. Faltermeier, M. Goldberg, M. Jones, A. Upham, D. Manger, G. Peterson, J. Lau, and A. E. Kaloyeros, Electrochem. Soc. 144, 1002 (1997).

[27]H. J. Lee, R. Sinclair, P. Li, and B. Roberts, J. Appl. Phys. 86, 3096 (1999).

[28]J. Musschoot, Q. Xie, D. Deduytsche, S. V. den Berghe, R. L. V. Meirhaeghe, and C. Detavrnier, Microelectron. Eng. 86, 72 (2009).

[29]A. M. Kia, J. Speulmanns, S. Bonhardt, J. Emara, K. Künel, N. Haufe, and W. Weinreich, Appl. Surf. Sci. 564, 150457 (2021).

[30]K. E. Elers, V. Saanila, P. J. Soininen, W. M. Li, J. T. Kostamo, S. Haukka, J. Juhanoja, and W. F. A. Besling, Chem. Vap. Deposition 8, 149 (2002).

[31]K. E. Elers, Doctoral Dissertation (University of Helsinki, Department of Chemistry, 2008).

[32]N. Samal, H. Du, R. Luberoff, K. Chetry, R. Bubber, A. Hayes, and A. Devasahayam, J. Vac. Sci. Technol. A 31, 01A137 (2013).

[33]G. B. Rayner, Jr., N. O'Toole, J. Shallenberger, and B. Johs, J. Vac. Sci. Technol. A 38, 062408 (2020).

[34]B. G. Kim et al., Appl. Surf. Sci. 541, 148482 (2021).

[35]C. H. Ahn, S. G. Cho, H. J. Lee, K. H. Park, and S. H. Jeong, Met. Mater. Int. 7, 621 (2001).

[36]J. Y. Kim, S. W. Seo, D. Y. Kim, H. T. Jeon, and Y. D. Kim, J. Vac. Sci. Technol. A 22, 8 (2003).

[37]Z. J. Ding, B. Zhu, W. J. Liu, X. H. Wu, and S. J. Ding, Jpn. J. Appl. Phys. 58, SHHA02 (2019).

[38]H. C. M. Knoops, L. Baggetto, E. Langereis, M. C. M. van de Sanden, J. H. Klootwijk, F. Roozeboom, R. A. H. Niessen, P. H. L. Notten, and W. M. M. Kessels, J. Electrochem. Soc. 155, G287 (2008).

[39]Y. J. Jang et al., J. Alloys Compd. 663, 651 (2016).

[40]Y. H. Joo, D. K. Nandi, R. Ramesh, Y. J. Jang, J. S. Bae, T. H. Cheon, and S. H. Kim, J. Alloys Compd. 858, 158314 (2021).

[41]B. Zhao, K. Sun, Z. Song, and J. Yang, Appl. Surf. Sci. 256, 6003 (2010).

[42]K. S. A. Butcher, V. Georgiev, and D. Georgieva, Coatings 11, 1506 (2021).

[43]D. R. Boris, M. J. Johnson, C. R. Eddy, Jr., and S. G. Walton, J. Vac. Sci. Technol. B 4, 044002 (2022).

[44]E. O. Filatova, S. S. Sakhonenkov, A. S. Konashuk, S. A. Kasatikov, and V. V. Afanas'ev, J. Phys. Chem. C 123, 22335 (2019).

[45]D. Jaeger and J. Patscheider, J. Electron Spectrosc. Relat. Phenom. 185, 523 (2012).

[46]G. R. Panghulan, M. R. Vasquez, Jr., Y. D. Edañol, N. Chanlek, and L. M. Payawan, Jr., J. Vac. Sci. Technol. B 38, 062203 (2020).

[47]D. Jaeger and J. Patscheider, Surf. Sci. Spectra 20, 1 (2013).

[48]See the supplementary material for the results of XRR, TEM, and RBS analysis of the TiN films, and a cross-sectional SEM image of the trench pattern used for the step coverage test.

19 March 2024 01:10:25